Civil Engineering Dimension
https://ced.petra.ac.id

Seismic Damage State Limits of Non-Engineered Buildings Considering the Randomness of Ground Motions

Kristiawan, S.A.[1]*, Sangadji, S.[1], Purwanto, E.[1], Safarizki, H.A.[2], Sulthon, A.H.A.[1], and Muflih, A.B.[1]
[1] Civil Engineering Department, Universitas Sebelas Maret, Jl. Ir. Sutami No. 36 A, Surakarta 57126, INDONESIA
[2] Civil Engineering Department, Universitas Veteran Bangun Nusantara, Jl. Letjend Sujono Humardani No. 1, Sukoharjo 57521, INDONESIA

DOI: https://doi.org/10.9744/ced.27.2.167-179

Article Info:
Submitted: Mar 08, 2025
Reviewed: Mar 26, 2025
Accepted: Aug 13, 2025

Keywords:
damage state,
incremental dynamic analysis,
non-engineered building,
randomness ground motions,
uncertainty.

Corresponding Author:
Kristiawan, S.A.
Civil Engineering Department,
Universitas Sebelas Maret, Jl. Ir. Sutami No. 36 A, Surakarta 57126, INDONESIA
Email: a.kristiawan@ft.uns.ac.id

Abstract

Earthquake-resistant structures are vital to achieving sustainable buildings as they minimize damage during seismic events and allow for easier repairs. In contrast, non-engineered buildings (NEBs) often suffer severe damage, contributing to waste that burdens the environment. Many residential buildings in Indonesia fall into this NEB category, so evaluating the extent of damage during earthquakes is essential. This study analyzed the seismic response of NEB using Incremental Dynamic Analysis (IDA). The dynamic pushover curves derived from the IDA were further examined to identify the damage limit states pertinent to NEB, considering the randomness of the ground motions. The proposed damage limit states, categorized into various levels (DS1-DS4) and their corresponding uncertainties due to random ground motions, highlight the vulnerability of NEBs to seismic events. The high probability of damage to NEBs makes stakeholders aware of the need to take measures to improve the resilience and, ultimately, the sustainability of residential buildings.

INTRODUCTION

Early disasters are among the most significant natural disasters and often result in catastrophic consequences for human safety, infrastructure, and the environment. Consequently, it is essential to implement tangible measures aimed at enhancing the resilience of regions vulnerable to seismic hazards [1,2]. Adopting building resilience practices has emerged as a key strategy for mitigating the risks associated with seismic events. Such buildings are designed to enhance resilience against disasters such as earthquakes and contribute to sustainable urban development [3]. These structures are engineered to withstand the forces generated by seismic activity, thereby significantly reducing the extent of damage and quickly recovering functionality [4]. Typical earthquake damage and failure can lead to substantial construction waste and further complicate the environmental challenges [5]. In contrast, resilient buildings prioritize designs that can endure these forces, thereby minimizing structural damage and waste generation. In addition, a significant advantage of resilient buildings is their ease of repair following earthquakes. Instead of total demolition, which can be economically burdensome and environmentally damaging, these structures are often restored with relative efficiency. This capability conserves resources, reduces waste, and fosters a more sustainable recovery process [6,7]. Sustainable buildings represent a forward-thinking solution that integrates sustainability principles with disaster resilience. They protect the lives of the inhabitants, safeguard the environment, and support local economies, ultimately cultivating a more resilient community in the face of the inevitable challenges posed by earthquakes.

Note : Discussion is expected before November, 1st 2025, and will be published in the "Civil Engineering Dimension", volume 28, number 1, March 2026.
ISSN : 1410-9530 print / 1979-570X online
Published by : **Petra Christian University**

In reality, many buildings do not follow the engineered requirements of earthquake-resistant design and therefore do not fulfill sustainability principles, making them vulnerable to damage and even collapse when an earthquake occurs. Most buildings that collapse or suffer damage from earthquakes or other disasters in Indonesian villages are residential buildings constructed without adhering to established standards; instead, they rely on personal experience. Many of these residential buildings in small towns and villages are based on traditional practices (non-engineered buildings), with designs adapted to local cultures and available materials [8]. Non-engineered buildings often do not comply with the technical regulations related to building design. Common issues include the use of substandard materials, inadequate reinforcement and detailing, and poor construction practices that negatively affect the overall quality of buildings [9]. The non-engineered conditions of these residential buildings raise concerns regarding their performance during earthquakes. Additionally, uncertainties frequently arise in determining the structural performance of such buildings owing to inadequate data used for the analysis. These uncertainties can originate from field measurements, structural model inconsistencies, or earthquake parameter variations employed in assessments [10].

The seismic performance of buildings can be evaluated using a fragility analysis. This analysis determines the probability of damage to a building based on the intensity of an earthquake and provides valuable insights into the potential risks and vulnerabilities associated with various seismic events [11]. A crucial step in evaluating the fragility of a structure is to accurately identify the damage states, which encompass a range of conditions from slight and moderate damage to extensive and complete failure [12]. The damage state criteria are outlined in FEMA P-58-1[13] and HAZUS MZ 2.1 [14] for various building types. Some studies have suggested quantifying these damage descriptions by linking them to engineering demand parameters such as story drift and drift ratio [15]. However, these damage descriptions and engineering demand parameters are primarily derived from the behavior of engineered buildings. Kristiawan et al. [9] demonstrated that the behavior of non-engineered buildings differs significantly from that of engineered structures. For example, in non-engineered buildings, compression failure often occurs before the reinforcement yields, which is attributed to the lower quality of the concrete used. Therefore, determining the damage states, ranging from slight to moderate, extensive, and complete, in non-engineered buildings should be based on their unique behaviors. Unfortunately, there is limited literature addressing this issue.

The input accelerogram simulating an earthquake affects the structural behavior identified through dynamic analysis. Consequently, the randomness of ground motion and modeling uncertainty can influence the evaluation of damage state limits [16,17]. A significant study by Vamvatsikos and Cornell [18] proposed the Incremental Dynamic Analysis (IDA), an effective methodology for seismic analysis, particularly for addressing the uncertainty related to ground motion. This method generates a series of IDA curves that depict how a structure behaves and performs across a range of conditions, from its elastic state through inelastic behavior, ultimately leading to total collapse under various ground motion intensities. Thus, an in-depth analysis of non-engineered building behavior concerning the progressive damage that occurs and the consideration of ground motion uncertainties is essential for determining the damage state limits of non-engineered buildings.

This study aims to determine the damage state limits of non-engineered buildings by considering the uncertainties associated with ground motion intensities. This case study focuses on a typical non-engineered residential building in Kendal Village in the Punung Subdistrict of the Pacitan Regency, Indonesia. This building serves as a typical residential dwelling in the local community, making it an ideal subject for this study. The findings of this research provide valuable insights for the fragility analysis of non-engineered residential structures. Specifically, they established a framework for damage-state limits and quantified the associated uncertainties, thus serving as a crucial reference point for future studies in this field.

BUILDING STRUCTURAL MODEL

The building under investigation is a single-story reinforced concrete portal with an earthen tile roof. The building area is 11.3 x 6 m2, while its height is 3.7 m. The compressive strength of the concrete components was measured at 4.53 MPa, indicating notably low-quality concrete. This may reflect insufficient skills among the workers tasked with mixing and producing concrete. The utilized steel reinforcements consisted of plain bars with a yield strength of 412 MPa. Figure 1 presents the floor plan of the structure and Figure 2 offers a detailed view of the cross-section of the reinforced concrete elements.

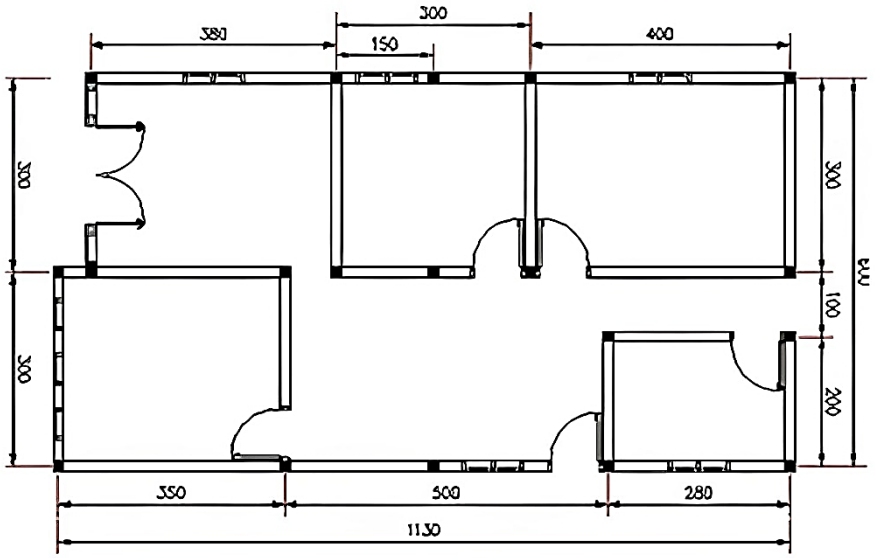

Figure 1. Building's Floor Plan

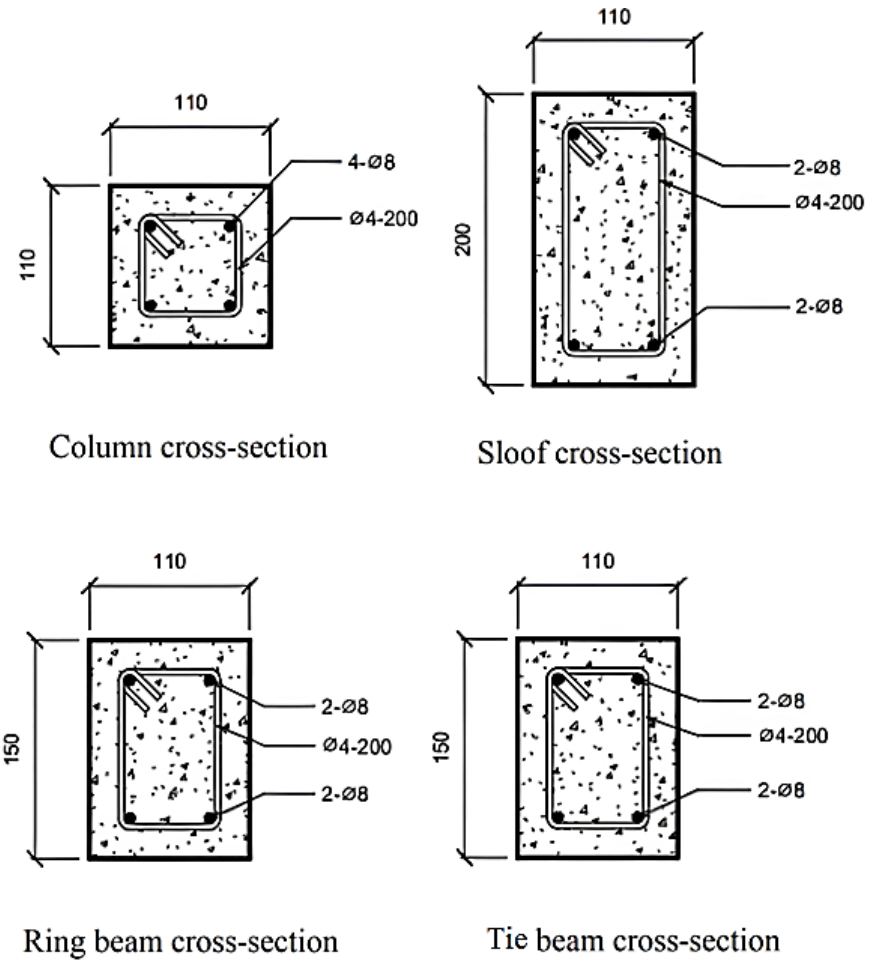

Figure 2. Reinforced Concrete Elements Detail

Incremental Dynamic Analysis

Superimposed Dead Load

When modeling a residential structure using SeismoStruct software, it is essential to consider the roof as a superimposed dead load. This necessitates the calculation of the roof load imposed on each ring beam element. This static load served as an additional dead load that was applied to the ring beam in the SeismoStruct environment.

Ground Motions Record

Throughout history, numerous ground motions resulting from significant earthquakes across the globe have been cataloged using accelerograms. These accelerograms effectively represent the ground acceleration plotted against time and provide valuable insights into the dynamics of these seismic events. The data derived from these accelerograms play a critical role in evaluating the seismic responses of structures. As outlined in SNI 1726:2019 [19], the best practices recommend that earthquake records employed for structural seismic assessments include a minimum of seven distinct accelerograms. Nevertheless, to effectively capture the uncertainties associated with the damage states arising from the variability in the structural responses, this study involved a random selection of 28 accelerograms. These were selected from a diverse array of earthquake records spanning various geographical locations, as listed in Table 1. This intentional random selection of ground motion records introduces uncertainty into the structural responses owing to the inherent variability among the records. The accelerogram data used in this study were obtained from the Pacific Earthquake Engineering Research Centre (PEERC) database (https://peer.berkeley.edu/research/databases), which is recognized for its extensive seismic data collection.

Table 1. Ground Motions Record used for this Study

No	Event	Station	Year	M (SR)
1	Loma Prieta RSN 731	APEEL 10 - Skyline	1989	6.93
2	Loma Prieta RSN 732	APEEL 10 - Skyline	1989	6.93
3	Loma Prieta RSN 733	APEEL 10 - Skyline	1989	6.93
4	Imperial Valley RSN 170	El Centro Array #9	1938	5
5	Imperial Valley RSN 172	El Centro Array #9	1938	5
6	Northridge RSN 5	Alhambra-Fremont School	1994	6.69
7	Northridge RSN 7	Alhambra-Fremont School	1994	6.69
8	San Fernando RSN 51	2516 Via Tejon PV	1971	6.61
9	San Fernando RSN 52	Anza Post Office	1971	6.61
10	Kern County RSN 12	LA-Hollywood Stor FF	1952	7.36
11	Kern County RSN 13	Pasadena-CIT Athenaeum	1952	7.36
12	Northern Calif 01	Ferndale City Hall	1941	6.40
13	Northern Calif 03	Ferndale City Hall	1954	6.50
14	Parkfield RSN 28	Cholame - Shandon Array #12	1966	6.19
15	Parkfield RSN 30	Cholame - Shandon Array #5	1966	6.19
16	Kobe RSN 1	Abeno	1995	6.90
17	Kobe RSN 2	Amagasaki	1995	6.90
18	Tabas Iran RSN 137	Bajestan	1978	7.35
19	Tabas Iran RSN 138	Boshrooyeh	1978	7.35
20	Nahanni Canada RSN 495	Site 1	1985	6.76
21	Nahanni Canada RSN 496	Site 2	1985	6.76
22	Montenegro RSN 4451	Bar-Skupstina Opstine	1979	7.10
23	Montenegro RSN 4452	Debar - Skupstina Opstine	1979	7.10
24	Kalamata RSN 565	Kalamata (BSMT)(1st trigger)	1986	5.40
25	Kalamata RSN 566	Kalamata (BSMT)(2nd trigger)	1986	5.40
26	San Francisco	Golden Gate Park	1957	5.28
27	El Alamo	El Centro Array #9	1956	6.80
28	Point Mugu	Port Hueneme	1973	5.65

Response Spectra

The residential building at the center of this study is a non-engineered structure located in Kendal Village within the Punung Subdistrict of the Pacitan Regency. This area is classified as having medium soil type (SD), which is a critical consideration in seismic studies. To evaluate the seismic characteristics of the site and its corresponding spectral acceleration parameters, we consulted the Indonesian earthquake map and adhered to the guidelines outlined in SNI 1726:2019 [19]. This building code provides comprehensive procedures for determining the target design spectral

acceleration response by considering specific site coefficient values and related spectral acceleration parameters. The results of our calculations, which detail the target spectral acceleration response explicitly tailored to the Pacific region, are presented in Figure 3.

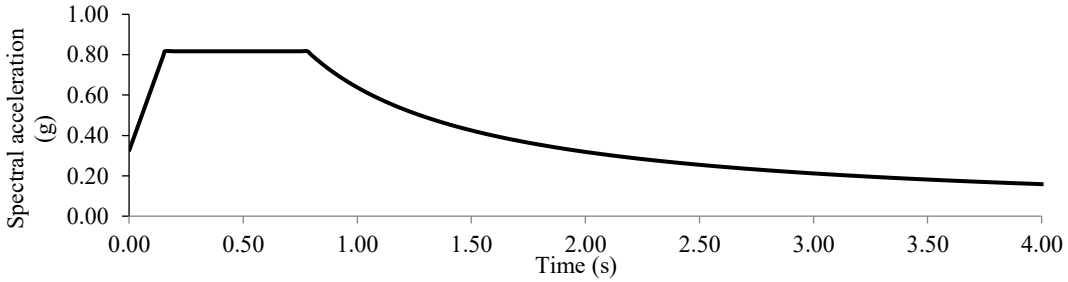

Figure 3. The Target Response Spectra of Pacitan

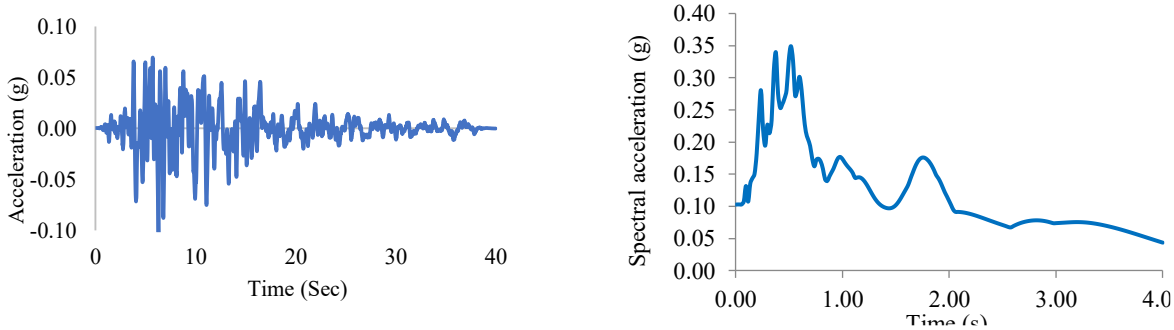

a. Accelerogram of Loma Prieta RSN 731 b. Response Spectra of Loma Prieta RSN 731

Figure 4. Generation of Response Spectra from the Accelerogram

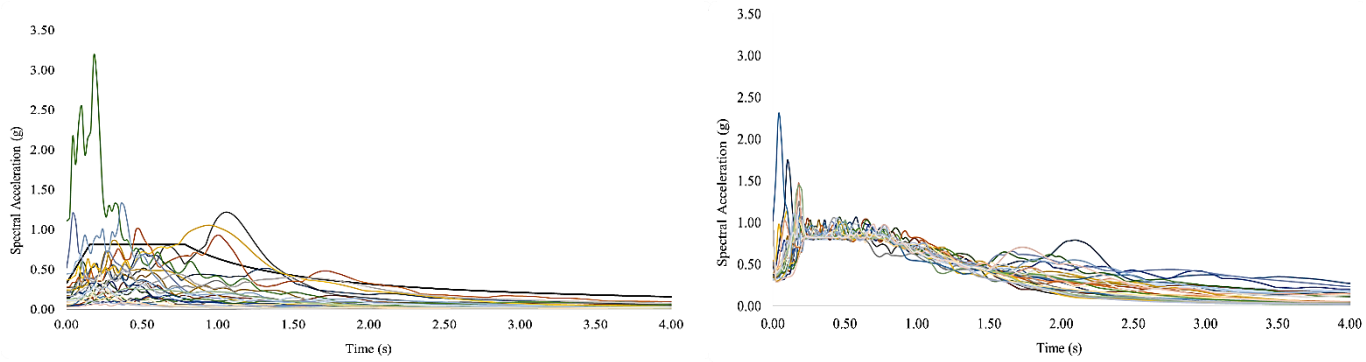

(a) Before Matching (b) After Matching

Figure 5. Matching the Response Spectra of Various Ground Motions to the Target Spectrum

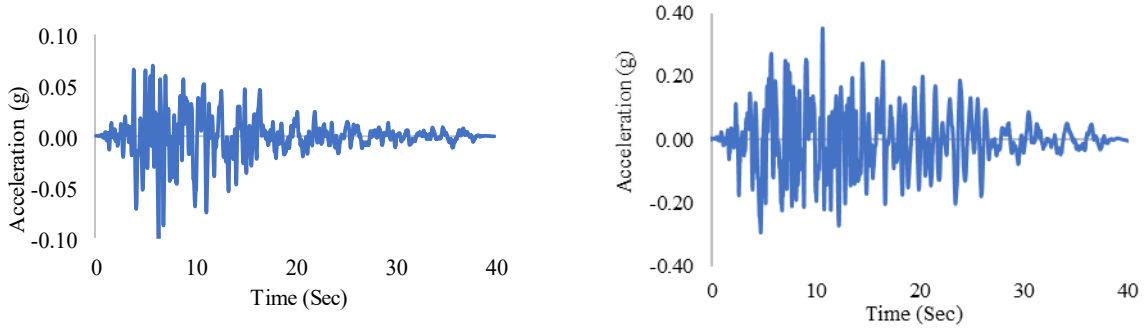

(a) Original Accelerogram (b) Artificial Accelerogram

Figure 6. Original and Artificial Accelerogram of Loma Prieta RSN 731

Initially, the ground motion records collected from various locations, as summarized in Table 1, were presented in a graphical format depicting acceleration versus time (accelerogram). These accelerograms were then transformed into

response spectra using SeismoMatch software. Figure 4 provides a clear example of this transformation, showing the response spectra derived from the accelerogram of the Loma Prieta RSN 731 earthquake. The resulting response spectra were compiled for the remaining ground motion records, as illustrated in Figure 5.a. It is important to note that the intensity levels of the earthquakes, as indicated by the response spectra from various locations, vary significantly from the target response spectra specific to the Pacitan area. To align these response spectra with the spectral response characteristics of Pacitan, an adjustment process was performed using SeismoMatch software, and the results are displayed in Figure 5.b. Following this adjustment, we derived the corresponding scale factors to create a matched accelerogram. This modified accelerogram, referred to as an artificial accelerogram, was used as the input for Incremental Dynamic Analysis (IDA). Figure 6 compares the original and artificial accelerograms for the Loma Prieta RSN 731 earthquake, highlighting the differences and adjustments made.

Modelling and Dynamic Analysis of Structure

Seismic analyses of non-engineered building structures were performed using Seismo-Struct software. The process commenced with the development of a detailed three-dimensional model of the building structure within the seismostructural environment, as depicted in Figure 7. In this analysis, we considered the self-weight of the structure and superimposed a fixed gravity load from the roof system, which acts as a dead load. The significance of this superimposed dead load was discussed in the previous subsection. A dynamic analysis of the building structure was carried out using the incremental dynamic method, which entails applying seismic loads in the form of ground motions, specifically through the use of an artificial accelerogram defined in an earlier section of this paper. This dynamic analysis represents a time history approach that investigates how a structure responds to increasing levels of seismic intensity over time. We began with a low intensity, where the structural response remained within the elastic range, and then gradually increased the intensity until a threshold capable of inducing collapse was reached. For this research, an incremental factor of 0.02 was chosen as the multiplier for the artificial accelerograms, facilitating a gradual escalation in seismic loading. SeismoStruct possesses features that automate the incremental dynamic analysis process, generating a dynamic pushover curve that graphically represents the envelope curve depicting the relationship between the base shear and the maximum structural response (measured as the top drift) for each increment of dynamic loading applied. This visualization enhances the understanding of the overall behavior of a structural system under simulated seismic events, offering valuable insights into its performance and vulnerability.

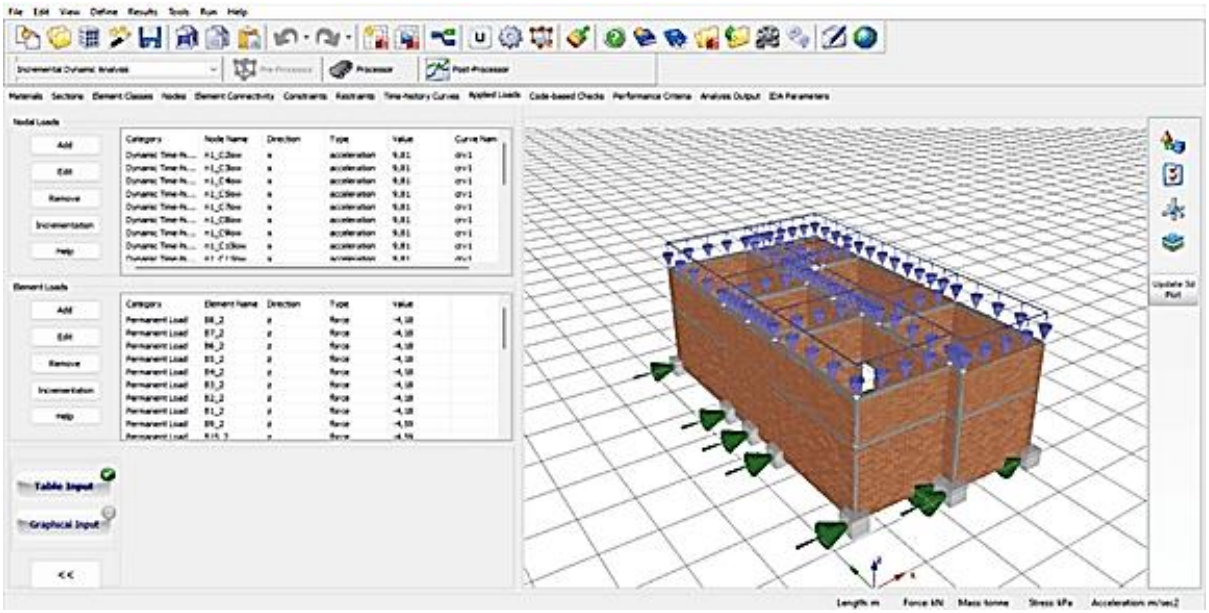

Figure 7. Modelling of the NEB in Seismostruct

RESULTS AND DISCUSSION

Determining Damage State from IDA Curves

The results of the incremental dynamic analysis performed on the NEB structure are illustrated by the dynamic pushover curves (capacity curves) in Figure 8. This curve provides a comprehensive overview of the relationship

between the magnitude of the base shear force and the corresponding peak displacement (drift) observed in non-engineered structures. The analysis incorporated multiple earthquake scenarios, and the resulting graphs consistently demonstrated behavioral patterns across the various conditions tested. The curves were also converted into the Acceleration-Displacement Response Spectrum (ADRS) format and are presented in Figure 9.

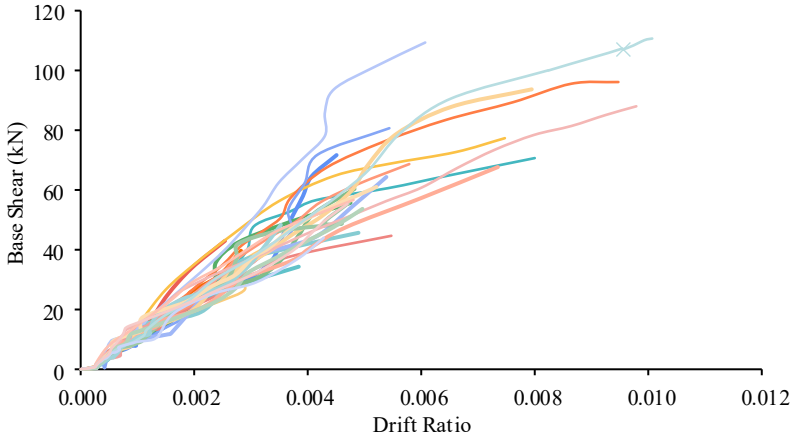

Figure 8. Capacity Curves of the Non-Engineered Structure

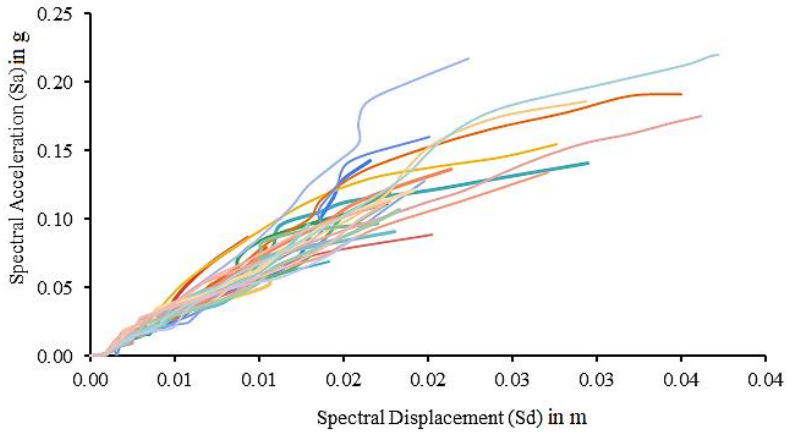

Figure 9. Capacity Spectrum (ADRS Format) Curves of the Non-engineered Structure

The damage experienced by a non-engineered structure due to seismic loads can be categorized into several stages, ranging from slight damage to complete damage and eventual collapse. This progression can be monitored through facilities in SeismoStruct. In this study, slight damage (DS1) is identified when surface cracks appear in the concrete, which occurs when the concrete strain reaches a value of -0.002. Following this cracking, an increase in the seismic load leads to the yielding of the reinforcement. At this stage, if one of the longitudinal reinforcements within the NEB structural elements initiated yielding, the overall structural system remained capable of bearing the earthquake load. Therefore, the condition in which the reinforcement first begins to yield is classified as a moderate level of damage (DS2). As the intensity of the earthquake continues to escalate, yielding of more reinforcements may occur, accompanied by increasingly severe damage as the confined concrete core begins to crack. This cracking takes place when the compressive strain in the concrete reaches -0.006, which defines this stage as extensive damage (DS3). If the earthquake load persists and increases further, the structure will ultimately become unstable, as evidenced by chord rotation. This condition is categorized as complete damage (DS4), preceding the eventual collapse of the building.

The determination of DS1-DS4, as outlined above, corresponds to the specific values of the base shear and drift ratio in the capacity curves (Figure 8) or spectral displacement (Sd) and spectral acceleration (Sa) in the capacity spectrum curves (Figure 9). Each curve reflects the response of the non-engineered structure when subjected to an earthquake of varying intensity, resulting in 28 corresponding values for DS1, DS2, DS3, and DS4. Table 2 summarizes the base shear and drift ratio values linked to each damage state, and Table 3 lists the corresponding spectral displacement (Sd) and spectral acceleration (Sa). The DS1-DS4 limit in this work differs from a previous study [9] that used the damage descriptions of FEMA-Hazus MH 2.1 [14] as a guideline. In a previous study, the drift ratios corresponding to DS1-DS4 were determined by interpreting the capacity curves and not by the defined values, as in this study.

Table 2. The Drift Ratio and Base Shear Corresponding to Various Damage State

Ground Motion Record	DS1		DS2		DS3		DS4	
	Drift ratio	Base shear (kN)	Drift ratio	Base shear (kN)	Drift ratio	Base shear (kN)	Drift ratio	Base shear (kN)
Loma Prieta RSN 731	0.0007	7.6211	0.0028	39.9210	0.0028	39.9210	0.0028	39.9210
Loma Prieta RSN 732	0.0007	8.2880	0.0030	48.3068	0.0037	53.1199	0.0054	61.0435
Loma Prieta RSN 733	0.0008	7.3194	0.0035	44.9841	0.0037	52.3200	0.0041	64.9156
Imperial Valley RSN 170	0.0006	7.5071	0.0025	43.4415	0.0025	43.4415	0.0025	43.4415
Imperial Valley RSN 172	0.0008	7.1543	0.0027	45.7522	0.0035	56.6216	0.0054	69.2210
Northridge RSN 5	0.0007	7.4571	0.0028	42.8454	0.0036	49.4337	0.0048	56.1867
Northridge RSN 7	0.0008	8.8839	0.0033	47.1636	0.0035	51.1479	0.0043	67.6556
San Fernando RSN 51	0.0007	9.0426	0.0038	34.7601	0.0038	34.7601	0.0038	34.7601
San Fernando RSN 52	0.0008	8.9345	0.0033	38.9116	0.0037	46.1254	0.0039	62.5266
Kern County RSN 12	0.0008	9.8136	0.0038	38.2473	0.0055	44.6097	0.0055	44.6097
Kern County RSN 13	0.0008	9.3045	0.0029	36.3569	0.0034	42.6956	0.0034	42.6956
Northern Calif 01	0.0009	9.4630	0.0031	30.6931	0.0035	36.2071	0.0041	52.3653
Northern Calif 03	0.0009	9.1262	0.0033	43.4471	0.0038	49.8365	0.0042	56.1308
Parkfield RSN 28	0.0006	8.6842	0.0034	36.1704	0.0049	45.9253	0.0049	45.9253
Parkfield RSN 30	0.0008	9.8646	0.0031	38.1953	0.0041	44.2323	0.0047	54.3597
Kobe RSN 1	0.0007	8.8818	0.0032	39.8694	0.0032	39.8694	0.0032	39.8694
Kobe RSN 2	0.0009	9.2139	0.0033	39.3547	0.0037	45.3514	0.0042	51.4332
Tabas Iran RSN 137	0.0010	9.0213	0.0028	42.0347	0.0035	46.3125	0.0043	48.9482
Tabas Iran RSN 138	0.0006	7.3582	0.0029	30.8873	0.0037	36.5621	0.0040	40.5913
Nahanni Canada RSN 495	0.0008	9.0342	0.0032	40.7561	0.0035	48.6920	0.0035	48.6920
Nahanni Canada RSN 496	0.0005	8.1655	0.0029	47.4821	0.0032	54.7882	0.0035	62.5206
Montenegro RSN 4451	0.0007	9.7610	0.0035	41.5673	0.0041	46.6664	0.0054	56.5132
Montenegro RSN 4452	0.0005	9.1759	0.0033	40.6936	0.0036	46.5940	0.0041	52.1459
Kalamata RSN 565	0.0007	8.0641	0.0029	32.6447	0.0034	37.5608	0.0044	47.9430
Kalamata RSN 566	0.0006	9.7937	0.0034	46.2034	0.0041	51.3902	0.0048	56.7472
San Francisco	0.0008	8.2826	0.0034	42.9262	0.0040	50.3966	0.0045	58.1842
El Alamo	0.0008	8.3006	0.0038	37.3342	0.0043	44.1272	0.0043	44.1272
Point Mugu	0.0006	7.6664	0.0034	36.1704	0.0038	40.6428	0.0038	40.6428
Average (μ)	**0.0007**	**8.6137**	**0.0032**	**40.2543**	**0.0037**	**45.6911**	**0.0042**	**51.5756**
Median (θ)	**0.0007**	**8.5740**	**0.0032**	**39.9786**	**0.0037**	**45.3435**	**0.0041**	**50.7880**

The analysis of the drift ratio limits revealed a notable disparity in the structural performance of non-engineered buildings compared to those designed under recognized standards. Specifically, the drift ratio values associated with various damage states in non-engineered structures (Table 2) are significantly lower than the thresholds proposed by FEMA's Hazus MH 2.1 [14] guidelines (see Table 4), particularly for buildings categorized as low-rise (< 6 m) and those utilizing reinforced concrete moment-resisting frame systems. Interestingly, even the damage thresholds set for these non-engineered buildings were inferior to those designed in the precode era, despite the latter not incorporating seismic design considerations. For instance, when exposed to a drift ratio of 0.005, a building constructed according to pre-code standards typically sustains only minor damage, which is classified as slight damage (DS1). In contrast, at the same drift ratio, a non-engineered building has already reached a critical failure point, experiencing damage categorized as DS4, indicating a complete level of damage. Nonetheless, the non-engineered building still exhibited a probability of surviving against collapse when subjected to a drift ratio of 0.005, as shown in Figure 8. An additional observation regarding the damage-state threshold values in non-engineered buildings is the close proximity between the time the reinforcement begins to yield (DS2) and the initiation of concrete core cracking (DS3). This phenomenon may occur because of the low quality of concrete used in non-engineered buildings, which can result in the failure of the concrete core before the yielding of the reinforcement can produce a ductile effect. This observation highlights the significant vulnerabilities associated with non-engineered buildings, including inadequate concrete quality, subpar reinforcement detailing, and other structural inadequacies, which contribute to the diminished performance of such buildings during seismic events.

Kristiawan et al. [20] conducted a comprehensive analysis of the behavior of reinforced concrete frame models based on the experimental tests conducted by Kakaletsis and Karayannis [21]. Their research focused on structural models representative of typical ductile concrete constructions, designed in accordance with established seismic codes. By employing finite element modeling techniques, Kristiawan et al. [20] identified various damage state limits relevant to these code-compliant structures. The study identified specific threshold values in terms of spectral displacement,

categorizing damage levels into four distinct states: slight damage at 0.09 meters, moderate damage at 0.19 meters, extensive damage at 0.33 meters, and complete damage at 0.70 meters. Notably, these values significantly exceeded the thresholds stipulated for non-engineered buildings (Table 3), highlighting the vulnerabilities inherent in non-engineered structures. Even at the minimal spectral displacement of 0.09 meters, where the code-compliant structure only sustains slight damage, the non-engineered building cannot survive (see Figure 9). This disparity is primarily attributable to the lack of ductile properties in non-engineered buildings, which do not benefit from the same level of structural resilience and design rigor that characterizes engineered structures adhering to seismic safety regulations. In this study, it is also noteworthy to compare the damage states of non-engineered buildings with the non-compliant structure outlined by Ahmad et al. [22]. Their non-compliant model features construction deficiencies, notably a concrete compressive strength of 13.80 MPa and the absence of confining ties in the beam-column joint panel zones. They identified five levels of damage, beginning with slight damage (LS1), characterized by the emergence of hairline flexural cracks at the top ends of the columns on the uppermost floor. Despite this slight damage, the structure remained fully operational following an earthquake. The next level, moderate damage (LS2), was indicated by the initiation of flexural cracks at the beam ends owing to the longitudinal bar slip. At this stage, the structure was operational. The following moderate damage is heavy damage (LS3), distinguished by the appearance of hairline cracks at joints lacking confining ties. The structure continues to function: Critical damage (LS4) occurred when the concrete cover began to spall from the joints with no confining ties, marking the point at which the structure reached the life safety level of service. The last level is incipient collapse (LS5), wherein the cover and core concrete spall from the non-tied joints, placing the structure on the verge of collapse. The limit values for these states, expressed as percentages of roof drift, were 0.23%, 0.60%, 0.82%, 1.48%, and 3.06% for LS1 through LS5, respectively. The non-compliant structure analyzed by Ahmad et al. was a two-story portal with a roof height of 7.316 m. Unfortunately, their study did not provide displacement data for the first floor, which prevented us from determining the magnitude of the interstory drift ratio. Consequently, the damage state limit of a non-compliant structure cannot be directly compared to that of a non-engineered building. However, suppose that the interstory drift is half the roof drift percentage. In this case, the data suggest that non-engineered buildings sustain more severe damage than non-compliant structures.

Table 3. The Spectral Displacement and Spectral Acceleration Corresponding to Various Damage State

Ground Motion Record	DS1		DS2		DS3		DS4	
	Sd (m)	Sa (g)	Sd (m)	Sa (g)	Sd (m)	Sa (g)	Sd (m)	Sa (g)
Loma Prieta RSN 731	0.00275	0.01510	0.01042	0.07908	0.01042	0.07908	0.01042	0.07908
Loma Prieta RSN 732	0.00269	0.01642	0.01128	0.09569	0.01358	0.10522	0.01996	0.12092
Loma Prieta RSN 733	0.00296	0.01450	0.01310	0.08910	0.01382	0.10364	0.01499	0.12859
Imperial Valley RSN 170	0.00232	0.01487	0.00931	0.08605	0.00931	0.08605	0.00931	0.08605
Imperial Valley RSN 172	0.00290	0.01417	0.00997	0.09063	0.01290	0.11216	0.02010	0.13711
Northridge RSN 5	0.00271	0.01477	0.01021	0.08487	0.01343	0.09792	0.01758	0.11130
Northridge RSN 7	0.00278	0.01760	0.01211	0.09342	0.01310	0.10131	0.01605	0.13401
San Fernando RSN 51	0.00264	0.01791	0.01416	0.06885	0.01416	0.06885	0.01416	0.06885
San Fernando RSN 52	0.00295	0.01770	0.01205	0.07708	0.01371	0.09137	0.01459	0.12385
Kern County RSN 12	0.00307	0.01944	0.01406	0.07576	0.02022	0.08836	0.02022	0.08836
Kern County RSN 13	0.00297	0.01843	0.01056	0.07202	0.01267	0.08457	0.01267	0.08457
Northern Calif 01	0.00335	0.01874	0.01140	0.06080	0.01289	0.07172	0.01517	0.10373
Northern Calif 03	0.00316	0.01808	0.01203	0.08606	0.01407	0.09872	0.01560	0.11118
Parkfield RSN 28	0.00235	0.01720	0.01034	0.07217	0.01801	0.09097	0.01801	0.09097
Parkfield RSN 30	0.00296	0.01954	0.01138	0.07566	0.01514	0.08762	0.01756	0.10768
Kobe RSN 1	0.00249	0.01759	0.01183	0.07897	0.01183	0.07897	0.01183	0.07897
Kobe RSN 2	0.00336	0.01825	0.01209	0.07795	0.01373	0.08983	0.01564	0.10188
Tabas Iran RSN 137	0.00362	0.01787	0.01023	0.08326	0.01290	0.09174	0.01582	0.09696
Tabas Iran RSN 138	0.00210	0.01458	0.01059	0.06118	0.01369	0.07242	0.01484	0.08040
Nahanni Canada RSN 495	0.00301	0.01789	0.01181	0.08073	0.01298	0.09645	0.01298	0.09645
Nahanni Canada RSN 496	0.00180	0.01617	0.01073	0.09405	0.01193	0.10853	0.01291	0.12384
Montenegro RSN 4451	0.00260	0.01933	0.01299	0.08234	0.01520	0.09244	0.01988	0.11194
Montenegro RSN 4452	0.00197	0.01818	0.01220	0.08061	0.01350	0.09229	0.01531	0.10329
Kalamata RSN 565	0.00244	0.01597	0.01085	0.06466	0.01263	0.07440	0.01643	0.09497
Kalamata RSN 566	0.00228	0.01940	0.01273	0.09152	0.01512	0.10179	0.01776	0.11241
San Francisco	0.00298	0.01641	0.01266	0.08503	0.01462	0.09983	0.01671	0.11525
El Alamo	0.00301	0.01644	0.01423	0.07395	0.01584	0.08741	0.01584	0.08741
Point Mugu	0.00212	0.01519	0.01273	0.07165	0.01404	0.08051	0.01404	0.08051
Average (μ)	**0.0027**	**0.0171**	**0.0117**	**0.0798**	**0.0138**	**0.0905**	**0.0156**	**0.1022**
Median (θ)	**0.0027**	**0.0170**	**0.0116**	**0.0792**	**0.0136**	**0.0898**	**0.0154**	**0.1006**

Table 4. Drift Ratio Limit Corresponding to Damage States

Seismic design level	Interstory drift ratio			
	Slight	Moderate	Extensive	Complete
High-code	0.0050	0.0100	0.0300	0.0800
Moderate-code	0.0050	0.0087	0.0233	0.0600
Low-code	0.0050	0.0080	0.0200	0.0500
Pre-code	0.0040	0.0064	0.0160	0.0400

The drift limits for confined masonry structures (unreinforced masonry supported by lightweight reinforced concrete frames) were examined by Vatteri and D'Ayala [23]. They established criteria for damage states based on three levels: Immediate Occupancy (IO), characterized by the development of flexural cracks; LS (Life Safety), which marks the threshold for major open cracks and wall panels disconnected from the confining frames or experiencing significant cracking; and Collapse Prevention (CP), indicated by the widespread development of major cracks leading to either local or global mechanisms. One method for determining the drift limit under specified limit states involves the generation of capacity curves. Their findings suggest that the IO, LS, and CP damage states occur when the confined masonry structure experiences drift in the ranges of 0.07-0.65%, 0.80-2.00%, and 1.27-5%, respectively. Given these figures, the non-engineered building analyzed in this study exhibited greater vulnerability to seismic events than the confined masonry structure.

A comparison of the damage state limits of non-engineered buildings examined in this study with those of other structure types, but not directly equivalent to the comparison, still offers valuable insights into the vulnerability of residential buildings in the Pacitan area of Indonesia during seismic events. This susceptibility prompted stakeholders to initiate efforts to improve the resilience of earthquake-prone regions. One significant initiative, led by Purwanto et al., proposed strengthening building joints to enhance the seismic performance of non-engineered structures. However, additional innovative strategies are necessary to reduce the risks of damage and potential collapse of these buildings.

Uncertainty of Damage States due to Randomness of Ground Motions

The response of a structure to earthquake loads involves various random variables, necessitating the introduction of structural uncertainty parameters to accommodate the inherent variability of these values. There are two key types of structural uncertainty: aleatoric uncertainty (βR) and epistemic uncertainty (βU). Aleatoric uncertainty arises from unpredictable random events, such as the response of a structure to random ground motions. However, epistemic uncertainty pertains to a limited understanding of natural phenomena. For instance, we often rely on specific assumptions in structural modeling because of the challenges in accurately representing the parameters and variables that reflect real-world conditions. The damage states outlined in Tables 2 and 3 offer a comprehensive perspective on how the values of the damage states vary owing to the inherent randomness of the ground motions. This variability is further illustrated in Figure 10, which presents the dispersion values for damage states DS1–DS4 along with their corresponding mean spectral displacement and acceleration values. Figure 10 shows a notable trend: as the damage level increased, the dispersion of the damage state values widened. This expanding dispersion underscores the heightened uncertainty in assessing damage states at high damage levels, highlighting the effects of unpredictable ground motion behavior on structural integrity.

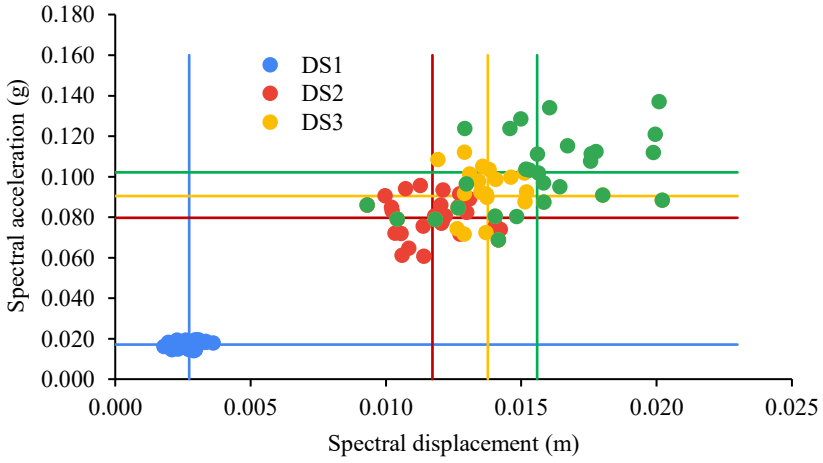

Figure 10. Dispersion of the Damage States due to Randomness of Ground Motions

Several studies have proposed methodologies for quantifying these uncertainties. This study employs Porter's model to assess the extent of aleatoric uncertainty in determining the damage states. Porter [24] introduced a formula to quantify uncertainty, represented as βR, which can be mathematically expressed as:

$$\beta R = \sqrt{\ln(1 + v^2)} \quad (1)$$

where v denotes the coefficient of variation associated with the damage state. Various parameters such as the drift ratio, spectral displacement, and acceleration can be utilized when evaluating the damage states in structures. By consulting Tables 2 and 3, one can apply this formula to calculate the value of βR, with the corresponding results compiled for clarity in Table 5. Notably, the uncertainty values derived from the drift ratio and spectral displacement parameters were similar. This is attributed to the fact that both parameters primarily represent the displacement characteristics of the structure itself. In contrast, spectral acceleration serves a different purpose, as it reflects the intensity measure, highlighting the variability in the structural response to seismic forces rather than displacement.

Table 5. Uncertainty of Damaged State due to Ground Motions

Damage State Parameter	Uncertainty due to ground motions (βR)			
	DS1	DS2	DS3	DS4
Drift ratio	0.160	0.110	0.149	0.177
Spectral displacement (m)	0.160	0.112	0.149	0.177
Spectral acceleration (g)	0.098	0.119	0.126	0.179

The βR values presented in Table 5 are notably lower than the thresholds recommended by FEMA P-695 [25], which indicates that record-to-record variability typically ranges from 0.20 to 0.40. This discrepancy may be attributed to the inherently fragile nature of non-engineered structures, as discussed in the previous section. It was emphasized that non-engineered structures are susceptible to significant damage, even at relatively low earthquake intensity levels. By contrast, engineered structures, despite being designed in the pre-code era, tend to sustain only minor damage at similar earthquake levels. This suggests a minimal probability that non-engineered structures can endure the predetermined damage state limit when subjected to earthquake loads at corresponding intensities.

CONCLUSIONS

The structural responses of non-engineered residential buildings were obtained as IDA curves from various ground motion input records. These responses allowed us to identify critical points corresponding to damage levels ranging from slight to complete. According to the damage state criteria established in this study, the threshold damage state values for non-engineered residential buildings in the Pacitan were notably lower than those for other structure types. Even during earthquake events that result in only slight damage to engineered buildings, non-engineered structures often experience complete damage. Moreover, the dispersion of the damage state values owing to the variability of the ground motion record was found to be lower than that of other building types. This suggests that the likelihood of non-engineered structures surviving within the specified damage-state limits is minimal. The high probability of failure of non-engineered buildings during earthquakes highlights the urgent need for stakeholders to implement preventive measures to enhance the resilience of these residential structures.

Acknowledgement

We would like to thank the parties involved in facilitating the field survey, especially PUPR Kabupaten Pacitan, which was a crucial phase of this study, for collecting data that depicted the building's non-engineered conditions.

Funding Statement

The research and publication of this article were made possible by financial support from the Ministry of Education, Culture, Research and Technology, Indonesia through the Hibah Fundamental (Contract No. 1076.1/UN27.22/PT. 01.03/2024).

Credit Authorship Contribution Statement

*** **Kristiawan**: Conceptualization, Formal analysis, Funding acquisition, Supervision, Writing – original draft. *** **Sangadji**: Supervision, Writing – review & editing *** **Purwanto**: Supervision, Investigation. *** **Safarizki**: Investigation, Writing – review & editing. *** **Sulthon**: Investigation, Formal analysis, Writing – original draft. *** **Muflih**: Investigation, Formal analysis, Writing – original draft.

Conflicts of Interest

The authors declare no conflicts of interest regarding this study.

Data Availability Statement

All data, models, or codes that support the findings of this study are available from the corresponding author upon reasonable request.

REFERENCES

1. Roohi, M., Ghasemi, S., Sediek, O., Jeon, H., Lindt, J.W. Van De, Shields, M., Hamideh, S., and Cutler, H., Multi-disciplinary Seismic Resilience Modeling for Developing Mitigation Policies and Recovery Planning, *Resilient Cities and Structures*, *3*(2), 2024, pp. 66–84. https://doi.org/10.1016/j.rcns.2024.07.003
2. You, T. and Tesfamariam, S., Spatial Correlation in Building Seismic Performance for Regional Resilience Assessment, *Resilient Cities and Structures*, *3*(2), 2024, pp. 57–65. https://doi.org/10.1016/j.rcns.2024.06.004
3. Kojima, K., Fujita, K., and Takewaki, I., Building Earthquake Resilience in Sustainable Cities in Terms of Input Energy, *Sustainable Cities and Society*, *12*, 2014, pp. 46–62. http://dx.doi.org/10.1016/j.scs.2014.01.004
4. Mohammadgholibeyki, N., Koliou, M., and Liel, A.B., Assessing Building's Post-Earthquake Functional Recovery Accounting for Utility System Disruption, *Resilient Cities and Structures*, *2*(3), 2023, pp. 53–73. https://doi.org/10.1016/j.rcns.2023.06.001
5. Bektas, N. and Jingjie, Z. Sustainable Waste Management Strategies for Earthquake Debris : Lessons from the 2008 China and 2023 Türkiye-Syria Disasters, *International Journal of Disaster Risk Reduction*, *116*(105153), 2025. doi:10.1016/j.ijdrr.2024.105153
6. Gao, C., Huang, L., Wang, L., Sun, Q., and Li, Y., Simulation and Numerical Analysis of the Seismic Performance of the Quick Repaired Seismic-Damaged RC Frame, *Soil Dynamics and Earthquake Engineering*, *188*(109083), 2025. https://doi.org/10.1016/j.soildyn.2024.109083
7. Cheng, S., He, H., Cheng, Y., and Sun, H., Seismic Resilience-Oriented Framework for the Optimal Repair Decision of Seismic-Damaged Structures, *Soil Dynamics and Earthquake Engineering*, *190*, 2025, pp. 109159. https://doi.org/10.1016/j.soildyn.2024.109159
8. Boen, T, *Earthquake Resistant Design of Non-Engineered Buildings In Indonesia*, retrieved from https://www.humanitarianlibrary.org/sites/default/files/2013/07/Indonesian Earthquake Resistant Design.pdf
9. Kristiawan, S.A., Safarizki, H.A., Purwanto, E., Sangadji, S., Trisnawan, A.D., and Nugroho, T.S., Damage State of Non-Engineered Residential Buildings owing to Earthquakes: A Case Study in Pacitan Regency, Indonesia, *Civil and Environmental Engineering, 20*(1), 2024. pp. 426–439. doi:10.2478/cee-2024-0033
10. Skoulidou, D. and Romão, X., Uncertainty Quantification of Fragility and Risk Estimates due to Seismic Input Variability and Capacity Model Uncertainty, *Engineering Structures*, *195*, 2019. pp. 425–437. https://doi.org/10.1016/j.engstruct.2019.05.067
11. Liu, C., Liu, B., Wang, X., Kong, J., and Gao, Y., Seismic Performance Target and Fragility of Masonry Infilled RC Frames under In-Plane Loading, *Buildings*, *12*(8), 2022. pp. 1–16, https://doi.org/10.3390/buildings12081175
12. Hapsari, I.R., Kristiawan, S.A., Sangadji, S., and Gan, B.S., Damage States Investigation of Infilled Frame Structure Based on Meso Modeling Approach, *Buildings, 13*(2), 2023 pp. 1–20. doi:10.3390/buildings13020298
13. FEMA P-58, *Seismic Performance Assessment of Buildings, Volume 1: Methodology*, Federal Emergency Management Agency (FEMA), 2018.
14. FEMA Hazus-MH 2.1, *Multi-hazard Loss Estimation Methodology, Earthquake Model, Hazus–MH 2.1: Technical Manual*, Federal Emergency Management Agency (FEMA), 2012.
15. Melani, A., Khare, R.K., Dhakal, R.P., and Mander, J.B., Seismic Risk Assessment of Low Rise RC Frame Structure, *Structures*, *5* , 2016, pp. 13–22. http://dx.doi.org/10.1016/j.istruc.2015.07.003
16. Hulsey, A.M., Sullivan, T.J., Horspool, N., Gerstenberger, M.C., and Elwood, K.J., Considering Uncertainty in the Collapse Fragility of New Zealand Buildings for Risk-Targeted Seismic Design, *Earthquake Engineering & Structural Dynamics*, *52*, 2023, pp. 4205–4221. doi:10.1002/eqe.3916
17. Nasrollahzadeh, K., Hariri-Ardebili, M.A., Kiani, H., and Mahdavi, G., An Integrated Sensitivity and Uncertainty Quantification of Fragility Functions in RC Frames, *Sustainability*, *14*(13082), 2022. https://doi.org/10.3390/ su142013082
18. Vamvatsikos, D. and Fragiadakis, M., Incremental Dynamic Analysis for Estimating Seismic Performance Sensitivity and Uncertainty, *Earthquake Engineering and Structural Dynamics*, *39*(2), 2010, pp. 141–163. doi:https://doi.org/10.1002/eqe.935

19. SNI 1726:2019, *Tata Cara Perencanaan Ketahanan Gempa untuk Struktur Bangunan Gedung dan Nongedung*, Badan Standarisasi Nasional Indonesia, 2019.
20. Kristiawan, S.A., Hapsari, I.R., Purwanto, E., and Marwahyudi, M., Evaluation of Damage Limit State for RC Frame based on FE Modeling, *Buildings*, *12*(1), 2022, pp. 1–22. doi:10.3390/buildings12010021
21. Kakaletsis, D.J. and Karayannis, C.G., Experimental Investigation of Infilled Reinforced Concrete Frames with Openings, *ACI Structural Journal, 106*(2), 2009, pp. 132–141. doi:10.14359/56351
22. Ahmad, N., Shahzad, A., Ali, Q., Rizwan, M., and Khan, A.N., Seismic Fragility Functions for Code Compliant and Non-Compliant RC SMRF Structures in Pakistan, *Bulletin of Earthquake Engineering, 16*(10), 2018, pp. 4675–4703. doi:10.1007/s10518-018-0377-x
23. Vatteri, A.P. and D'Ayala, D., Classification and Seismic Fragility Assessment of Confined Masonry School Buildings, *Bulletin of Earthquake Engineering*, *19*(5), 2021, pp. 2213–2263. https://doi.org/10.1007/s10518-021-01061-9
24. Porter, K.A, *Beginner's Guide to Fragility, Vulnerabilit, and Risk*, Springer Berlin Heidelberg, 2021.
25. FEMA P695, *Quantification of Building Seismic Performance Factors*, Federal Emergency Management Agency (FEMA), 2009.